Supporting Information

Lu et al. 10.1073/pnas.1200506109

SI Materials and Methods

Anesthesia was induced with 3% isoflurane followed by intramuscular administration of the α_2-agonist (dexmedetomidine; 0.015 mg/kg). Rats were then positioned into a customized holder. During initial scanning, isoflurane (1%) in oxygen-enriched air was delivered via a customized MRI-compatible nose cone with continuous intramuscular infusion of dexmedetomidine (0.03 $mg \cdot kg^{-1} \cdot h^{-1}$) using an infusion pump. A noninvasive pulse oximeter (Starr Life Sciences) was connected to the hind paw to continuously monitor arterial oxygen saturation, which was maintained above 96% by adjusting the oxygen concentration in the gas mixture. Cardiac and respiration rates were continuously monitored. Core body temperature was maintained at 37.5 ± 0.3 °C using a water-circulating heating pump. Two needle electrodes were inserted into the right forepaw between digits 2 and 3 and digits 4 and 5 and connected to a constant-current stimulator (model S88; Grass Instruments). Stimulation parameters were 3-ms pulse width, 1-mA current at a frequency of 9 Hz (1). After the anatomical localization scans were acquired, isoflurane concentration was reduced to 0.25%. The typical respiration rate ranged from 45 beats per minute (bpm) when the scan started and gradually increased to 70–85 bpm. In some cases, when the respiration rate increased to 90 bpm, isoflurane was adjusted to 0.5%.

Resting State Functional MRI in Control Rats. Animal MRI experiments were performed on a Bruker Biospin 9.4T scanner (Bruker Medizintechnik). A volume coil was used for radio frequency (RF) excitation, and a circular surface coil was used for signal reception. High-resolution T_2-weighted anatomical images were acquired using a rapid acquisition with relaxation enhancement (RARE) sequence [repetition time (TR) = 2,000 ms, effective echo time (TE) = 50 ms, RARE factor = 8]. Anterior commissure [−0.36 mm from bregma (2)] appears dark in T_2-weighted images, and was used as the landmark to localize slices.

In addition to the above physiological monitoring, we assessed the functional status of the brain under the above anesthetic regime by measuring the functional MRI (fMRI) responses to electrical forepaw stimulation. This was performed in a pilot study using a separate group of animals (n = 11). The stimulation paradigm was a block design consisting of three alternating cycles of 30 s ON/30 s OFF, starting with a 20-s baseline, for a total of 200 s. This was repeated every 15 min for about 4.5 h. Each rat in the pilot group was studied on two occasions separated by 1 wk.

After determining that the optimum experimental window for stable evoked blood oxygenation level-dependent (BOLD) responses began about 90 min after the initiation of dexmedetomidine infusion (Fig. S1), we performed a series of resting state fMRI scans on a second group of animals (n = 16) using a single-shot gradient-echo echo-planar imaging (EPI) sequence. Scan parameters were: field of view (FOV) = 3.5 cm, matrix size = 64 × 64, TE = 15 ms, and TR = 1000 ms, 11 slices with a thickness of 1 mm. We collected 260 volumes of images during each session, with a total of 119 scan sessions from the 16 animals.

Data Analysis. ***Identification of rat default mode network.*** Geometric distortions in EPI images were corrected using the PLACE method (3). Data preprocessing included slice-timing correction, linear and quadratic trend removal, and spatial smoothing with a Gaussian kernel (full width at half maximum = 0.6 mm). Images from individual animals were then coregistered onto a common 3D space aligned with rat stereotaxic atlas using an approach previously described (4, 5). Analyses were performed within the AFNI framework (6).

Given that the purpose of the forepaw stimulation experiment was to evaluate the fMRI signal consistency across the 4.5-h experimental period, we calculated fractional signal changes between the ON and OFF periods and parsed the experimental duration into five time windows following dexmedetomidine induction: I: 0–30 min; II: 30–90 min; III: 90–150 min; IV: 150–210; and V: 210–270 min. Window I corresponds to the time when anatomical localization scans and magnetic field shimming were finished and the first two electrical forepaw stimulation scans were performed. During each of the subsequent 1-h windows, three forepaw stimulation runs were performed separated by 15-min rest intervals. BOLD signal within an individual time window was averaged. Region of interest analysis was performed in voxels within a common activation map and subjected to a one-way ANOVA across the five time windows. A $P < 0.05$ with a minimum cluster size of 8 voxels was considered significant. A subsequent two-way ANOVA (time window × week) was performed to identify consistency of the response.

Resting state fMRI data were analyzed using group-level independent component analysis (ICA) within the FSL software package (http://www.fmrib.ox.ac.uk/fsl/melodic/index.html) (7). The number of components was set to 30. To evaluate the robustness of the component maps identified by ICA, we performed follow-up analyses by setting the number of components to 20 and 40. Between-subject analysis and group statistical comparison were conducted using the dual-regression approach (8), which involves the following two linear regression steps: First, individual spatial component maps derived from group ICA were regressed against each volume of fMRI data; the resulting spatial regression coefficients were concatenated across time. Second, the variance-normalized time series from the above spatial regressions were regressed against the corresponding resting state fMRI time course to estimate the regression weights of specific component maps in individual animals. For each animal, the regression weight maps corresponding to the same group ICA component were averaged across the two scan sessions. Results from all 16 animals were then subject to one-sample t test against zero. A threshold of $t > 5.6$ with the corrected $P < 0.05$ (uncorrected $P < 5 \times 10^{-5}$) was applied to generate final maps for each group ICA component. Component maps were coregistered to a high-resolution rat digital atlas to aid in structural identification (5).

Network analysis of rat default mode network. Thirteen a priori regions of interest (ROIs) were chosen based on the anatomical structures comprising the network. Pearson correlation coefficients of the average time courses between each ROI pair were computed and subjected to one-sample t tests against zero after z transformation. A Bonferroni-corrected significance level of $P < 0.0005$ was used to threshold the correlation matrix into a binarized matrix (S = 38.5%; the sparsity, S, of a network is the ratio of the number of existing edges and possible maximum edges in the network) whose element is 1 if there is significant correlation between two brain regions and 0 otherwise. The degree of each ROI was calculated and the ROIs with the highest degree were considered as network hubs.

Network modularity was identified as follows: The modularity $Q(p)$ for a given partition (p) of the brain functional network is defined as (9)

$$Q(p) = \sum_{s=1}^{N_M} \left[\frac{l_s}{L} - \left(\frac{d_s}{2L} \right)^2 \right],$$

where N_M is the number of modules, L is the number of connections in the network, l_s is the number of connections between nodes in module s, and d_s is the sum of the degrees of the nodes in module s. The modularity index quantifies the difference between the number of intramodule links of actual network and that of random network in which connections are linked at random. The aim of this module identification process is to find a specific partition (p) that yields the largest network modularity, $Q(p)$. Nonlinear optimization using the simulated annealing approach was used to find the partition (10).

Human resting state fMRI data acquisition and analysis. Thirty-nine healthy human subjects were recruited under a protocol approved by the Institutional Review Board of the National Institute on Drug Abuse Intramural Research Program. Signed informed consents were obtained from all participants before study enrollment. Subjects were excluded if they had any major illness or a history of neurological or psychiatric disorders. fMRI data were collected on a 3T Allegra MR scanner (Siemens) equipped with a quadrature volume head coil. Head movement was minimized by using a polyurethane foam helmet individually made for each participant. During the 6-min resting scan, participants were instructed to keep their eyes closed and not to think of anything in particular. Thirty-nine 4-mm-thick slices parallel to the anterior-posterior commissure without an interslice gap were prescribed to cover the whole brain. The resting data were acquired using a single-shot gradient-echo EPI sequence with a TR of 2 s, TE of 27 ms, flip angle (FA) of 77°, FOV of 220 × 220 mm, and in-plane resolution of 3.44 × 3.44 mm. For registration purposes, high-resolution anatomical images were acquired using a 3D magnetization prepared rapid gradient-echo (MPRAGE) T_1-weighted sequence with a TR of 2.5 s, TE of 4.38 ms, FA of 7°, and voxel size of 1 × 1 × 1 mm.

Data preprocessing before ICA analysis was conducted in AFNI (6). Preprocessing included slice-timing correction, motion correction, spatial normalization to the standard Talairach space with a resampled resolution of 3 × 3 × 3 mm^3, spatial smoothing with a 6-mm Gaussian kernel, and quadratic detrending. To further align the resting state functional data across subjects, an unbiased group-wise nonlinear registration method was used to deform each spatially smoothed image to an implicit group reference image based on a small deformation elastic model (11). Each subject's dataset was then concatenated temporally, and the concatenated dataset was fed into the ICA algorithm implemented in MELODIC within the FSL software package (7) to generate 20 component maps.

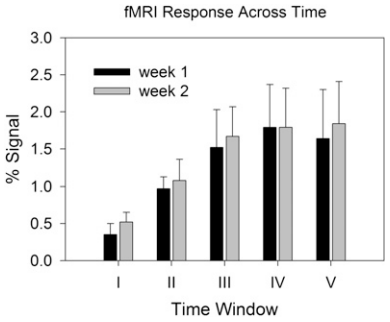

Fig. S1. fMRI response across the 4.5-h experimental period (n = 11). The five time windows were classified based on the time following dexmedetomidine induction (I: 0–30 min; II: 30–90 min; III: 90–150 min; IV: 150–210; V: 210–270 min). Window I corresponds to the time when slice localization scans were finished and the first two electrical forepaw stimulation scans were performed. Data are mean ± SD. Note similar fMRI responses in time windows III–V, which were significantly greater than in time windows I and II ($P < 0.02$). Also note similar fMRI responses in weeks 1 and 2 ($P > 0.07$). These data suggest consistent fMRI responses in the last three experimental windows, presumably because anesthesia levels and physiological parameters reached stable, steady-state conditions.

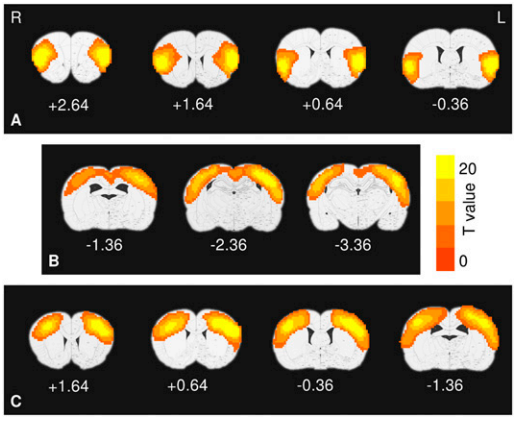

Fig. S2. Functional connectivity maps identified by ICA. The centers of the clusters are localized in the insular cortex (*A*), primary somatosensory cortex in the whisker barrel region (S1BF) (*B*), and forelimb region (S1FL) (*C*). Numbers are coordinates (in mm) relative to bregma. L, left; R, right.

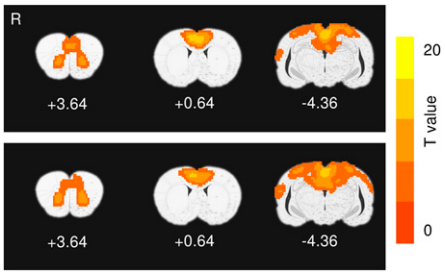

Fig. S3. Default mode network (DMN) identified by group ICA with a total of 20 (*Upper*) and 40 (*Lower*) independent components (ICs). Note similar spatial patterns despite different ICs specified, demonstrating the presence of a robust DMN in the rat brain. Electrical forepaw stimulation, a task that requires minimal cognitive load, did not modulate the connectivity patterns.

1. Zhao F, Zhao T, Zhou L, Wu Q, Hu X (2008) BOLD study of stimulation-induced neural activity and resting-state connectivity in medetomidine-sedated rat. *Neuroimage* 39:248–260.
2. Paxinos G, Watson C (2007) *The Rat Brain in Stereotaxic Coordinates* (Elsevier, San Diego), 6th Ed.
3. Xiang QS, Ye FQ (2007) Correction for geometric distortion and N/2 ghosting in EPI by phase labeling for additional coordinate encoding (PLACE). *Magn Reson Med* 57:731–741.
4. Lu H, et al. (2007) Cocaine-induced brain activation detected by dynamic manganese-enhanced magnetic resonance imaging (MEMRI). *Proc Natl Acad Sci USA* 104:2489–2494.
5. Lu H, et al. (2010) Registering and analyzing rat fMRI data in the stereotaxic framework by exploiting intrinsic anatomical features. *Magn Reson Imaging* 28:146–152.
6. Cox RW (1996) AFNI: Software for analysis and visualization of functional magnetic resonance neuroimages. *Comput Biomed Res* 29:162–173.
7. Beckmann CF, DeLuca M, Devlin JT, Smith SM (2005) Investigations into resting-state connectivity using independent component analysis. *Philos Trans R Soc Lond B Biol Sci* 360: 1001–1013.
8. Beckmann CF, Mackay CE, Filippini N, Smith SM (2009) Group comparison of resting-state FMRI data using multi-subject ICA and dual regression. *Neuroimage* 47:2.
9. Newman ME, Girvan M (2004) Finding and evaluating community structure in networks. *Phys Rev E Stat Nonlin Soft Matter Phys* 69:026113.
10. Guimerà R, Sales-Pardo M, Amaral LA (2004) Modularity from fluctuations in random graphs and complex networks. *Phys Rev E Stat Nonlin Soft Matter Phys* 70:025101.
11. Geng X, Christensen GE, Gu H, Ross TJ, Yang Y (2009) Implicit reference-based group-wise image registration and its application to structural and functional MRI. *Neuroimage* 47: 1341–1351.

Table S1. Major sensory and limbic afferents to areas involved in rat DMN

	Sensory afferents	Limbic afferents
Orbital medial prefrontal cortex (MO, VO, LO, PrL)	Olfactory (piriform cortex, anterior olfactory nucleus)	Perirhinal cortex
	Gustatory	Amygdala
	General visceral	
	Visual (OC2M, OC2L)	
	Somatosensory (Par1, Par2)	
Anterior cingulate cortex (CG1, CG2)	Visual (OC1, OC2M)	Hippocampus
	Auditory (TeA)	Perirhinal cortex, entorhinal cortex, basolateral amygdala
Posterior parietal cortex (PPC)	Somatosensory (Par1, Par2)	Perirhinal cortex
	Visual (OC2M, OC2L)	
	Auditory (Te1)	
Rostrosplenial cortex (RSD/RSG)	Visual (OC2M, OC2L)	Hippocampus
		Perirhinal cortex
Temporal association cortex	Auditory (Te1)	Perirhinal cortex
	Visual (OC1, OC2M, OC2L)	Basolateral nuclei of the amygdala

The list of the afferents is based on refs. 1–8. ACC, anterior cingulate cortex; CG1/CG2, cingulate cortex area 1 and 2; mPFC, medial prefrontal cortex; OC1, OC2M, and OC2L, primary, medial, and lateral secondary occipital areas; Par1 and Par2, primary and secondary parietal area; PrL, rostral dorsal prelimbic cortex; PtPR and PtPD, rostral and dorsal posterior parietal cortex; RSG/RSD, retrosplenial granular and dysgranular cortex; Te1, primary temporal cortex; TeA, temporal association cortex; V2M, medial secondary visual cortex; VO, LO, and rMO, ventral, lateral, and rostral medial orbital cortex.

1. Vogt BA, Miller MW (1983) Cortical connections between rat cingulate cortex and visual, motor, and postsubicular cortices. *J Comp Neurol* 216:192–210.
2. Reep RL, Corwin JV, King V (1996) Neuronal connections of orbital cortex in rats: Topography of cortical and thalamic afferents. *Exp Brain Res* 111:215–232.
3. Reep RL, Chandler HC, King V, Corwin JV (1994) Rat posterior parietal cortex: Topography of corticocortical and thalamic connections. *Exp Brain Res* 100:67–84.
4. Condé F, Audinat E, Maire-Lepoivre E, Crépel F (1990) Afferent connections of the medial frontal cortex of the rat. A study using retrograde transport of fluorescent dyes. I. Thalamic afferents. *Brain Res Bull* 24:341–354.
5. Deacon TW, Eichenbaum H, Rosenberg P, Eckmann KW (1983) Afferent connections of the perirhinal cortex in the rat. *J Comp Neurol* 220:168–190.
6. Heidbreder CA, Groenewegen HJ (2003) The medial prefrontal cortex in the rat: Evidence for a dorso-ventral distinction based upon functional and anatomical characteristics. *Neurosci Biobehav Rev* 27:555–579.
7. Allen GV, Saper CB, Hurley KM, Cechetto DF (1991) Organization of visceral and limbic connections in the insular cortex of the rat. *J Comp Neurol* 311:1–16.
8. Vaudano E, Legg CR, Glickstein M (1991) Afferent and efferent connections of temporal association cortex in the rat: A horseradish peroxidase study. *Eur J Neurosci* 3:317–330.

Table S2. Major anatomical connections among areas of rat DMN

	OMPFC (MO, VO, LO, PrL)	ACC	PPC	RSC	TeA	Hippo
OMPFC	-	← →	← →			
ACC		-	PPC→ACC	← →		ACC→Hippo
PPC			-	← →		
RSC				-		← →
TeA	TeA→PrL	TeA→ACC		TeA→RSC	-	
Hippo	Hippo→MO, PrL					-

Arrows → and ← indicate directions of projections. See refs. 1–8 in the legend for Table S1. OMPFC, orbital medial prefrontal cortex; RSC, retrosplenial cortex (granular and dysgranular).